Sci. Rep. Kanazawa Univ.
Vol.58, pp.13-29, 2014

Measurement of whole-rock trace-element composition of Cr-rich rocks on fused glass by LA-ICP-MS: data reliability of chromite-bearing fused glass

Akihiro TAMURA*, Norikatsu AKIZAWA and Shoji ARAI

Department of Earth Sciences, Kanazawa University: Kakuma, Kanazawa 920-1192, Japan

* *Corresponding author* Email : aking826@staff.kanazawa-u.ac.jp

(Received January 14, 2015 and accepted in revised form February 16, 2015)

Abstract Information from whole-rock trace-element compositions is significant for petrological studies. LA-ICP-MS technique can rapidly determine whole-rock trace-element compositions by fused glasses prepared by homogenization of rock powders. As already reported, several trace-element abundance (Sc, Ti, V, Cr, Co, Ni, Rb, Sr, Y, Zr, Nb, Ba, Th and REEs) of basaltic and andesitic rocks can be determined with high accuracy by the routine measurement on the flux-free fused glass using LA-ICP-MS in our laboratory. In this study, based on the previous report, whole-rock trace-element compositions of some Cr-rich rocks, mantle diopsidite and related rocks from the Oman ophiolite, were determined by the routine work. The mantle diopsidite is locally rich in chromite and its fused glass prepared includes quench crystals and residual grains of chromite. Here, we assessed the reliability and uncertainty of our data obtained from such incompletely homogenized fused glasses. High precision of 3-spot analyses supports that quench crystals of chromite were homogeneously distributed in the fused glass. This suggests that the analytical data obtained from spots unrelated to residual chromite grains are reliable for whole-rock trace-element compositions. The heterogeneity caused by residual chromite grains can be ignored in the measurement of incompatible elements (Sr, Y, Zr, and REEs). Our analytical results of 6 fused glass beads prepared from the diopsidite samples indicate that heterogeneity of the mantle diopsidite in terms of the abundance of chromite is scarcely reflected by incompatible-element compositions while the heterogeneity is clearly characterized by Cr abundance.

Keywords: LA–ICP–MS, fused glass, direct fusion, REE, diopsidite

1 Introduction

Whole-rock compositions are essential for describing and discussing petrographical characteristics of various geological samples, especially volcanic rocks. X-ray fluorescence (XRF) and inductively coupled plasma mass spectrometry (ICP-MS) analyses are widely used for determining major- and trace-element abundances of the samples, respectively. In petrological studies, abundances of trace elements represented by "incompatible elements", such as rare earth elements (REE), high-field strength elements (HFSE) and large ion lithophile elements (LILE), are useful as a tool for detailed discrimination of magma or rocks and are used in numerical modeling for their evolution processes (e.g., Sun and McDonough, 1989; Shaw, 2006; Pearce, 2008).

The trace-element analysis is conventionally carried out by a solution prepared from rock samples with annoying acid dissolution procedures. Further techniques, like microwaves and pressure bombs, are often necessary to complete digestion of insoluble refractory minerals, for example, zircon or chromite (e.g., Eggins et al., 1997). Laser-ablation technique combined with ICP-MS (LA-ICP-MS) is recently well established to determine in-situ trace-element compositions of rock-forming minerals and glasses (e.g., Eggins et al., 1998; Mason et al., 1999; Sylvester, 2001a; Tamura et al., 2008; Hirano et al., 2013). The technique has been applied for whole-rock analysis by preparing homogenized target materials, such as pressed-powder pellet and fused glass (Fedrowich et al., 1993; Jarvis and Williams, 1993; Sylvester, 2001b; Eggins, 2003; Orihashi and Hirata, 2003; Nehring et al., 2008; Stoll et al., 2008; Ito et al., 2009; Zhu et al., 2013; Garbe-Schönberg and Müller, 2014; Tamura et al., 2015 in press). Pressed-powder pellet is the simplest way for the whole-rock analysis although individual powder grains often cause heterogeneity at target position. The fused glass prepared by mixing with flux (lithium borate) is another way (Eggins, 2003), but the elemental contamination from the flux, and memory effect of Li and B interferes with the ICP-MS analysis. Preparation of flux-free fused glass is also simple and rapid way for LA-ICP-MS analysis (e.g., Fedrowich et al., 1993; Stoll et al., 2008; Tamura et al., 2015 in press). However, loss of the volatile elements during preparation is more serious in this method than in the flux-using method because of higher temperature conditions of melting for the former. Furthermore, highly refractory minerals, such as chromite as in the solution preparation, could not be completely decomposed in fusing. Therefore, the residual chromite may cause the modal heterogeneity in the fused glass. Heterogenous distribution of Cr in a flux-free fused glass was reported by in-situ analysis and this was considered to be derived from uneven formation of chromite as a quench phase during the vitrification (e.g., Jochum et al., 2000). Nevertheless the heterogeneity of Cr in the fused glass, the whole-rock incompatible-element compositions has been accurately determined by LA-ICP-MS analysis (e.g., Fedrowich et al., 1993; Stoll et al., 2008;

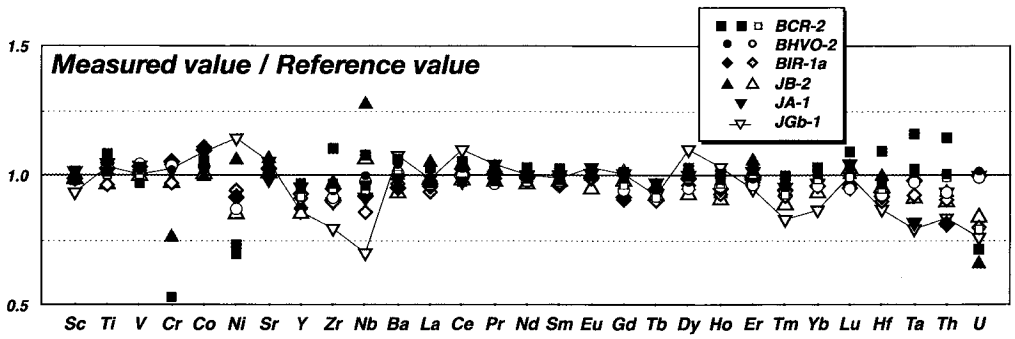

Figure 1. Accuracy of whole-rock trace-element measurements using the fused glass and LA-ICP-MS in our laboratory (data from Tamura et al., 2015 in press). The fused glass was prepared from USGS and GSJ powdered geological reference materials of basaltic-andesitic compositions. Measured values are mean value of 3-spot analyses of the fused glass. The reference values are from GeoReM database and the literature (see Tamura et al., 2015 in press).

Tamura et al., 2015 in press).

Our previous study demonstrated vitrification procedure of powdered rock samples, such as a "flux-free fused glass method", and the LA-ICP-MS analysis of products as a rapid routine measurement work in our laboratory (Tamura et al., 2015 in press). We successfully obtained visibly homogeneous glass beads of basaltic and andesitic rock samples. We also showed that, by 3-spot analysis of the fused glass, many incompatible elements can be accurately and precisely determined in spite of Cr heterogeneity of exceeding 20% in precision. Relatively high Cr-abundance samples (>280μg/g; e.g., BHVO-2 and BIR-1a) can be also reproduced within 15% accuracy (Fig. 1). However, a homogeneous flux-free fused glass is hardly created from extremely Cr-rich rocks because quench and residual crystals of chromite are frequently produced in the melting and vitrification. Such heterogeneities of the fused glass probably cause further uncertainties in the spot analysis by LA-ICP-MS. Here, we report the preparation of fused glass from an extremely Cr-rich rock sample and the analysis for whole-rock trace -element compositions. We discuss their reliability and uncertainty of data obtained from chromite-bearing "heterogeneous" fused glass to show their usefulness as the source of information of incompatible elements for petrological study.

2 Samples

A diopsidite sample from the mantle section of the Oman ophiolite was used in this study. The "mantle diopsidite" is mainly composed of diopside with accessory chromite. To consider the macro-scale modal heterogeneity of the diopsidite, the chromite-concentrated (chromite-rich diopsidite) and chromite-poor portions (chromite-poor

Table 1. Whole-rock major-element compositions (in wt%) of studied samples

Rock	Mantle diopsidite		Whitish Rock	Gabbro
Sample	chromite-rich diopsidite	chromite-poor diopsidite		
SiO_2	46.36	50.36	55.78	49.25
TiO_2	0.08	0.06	0.07	0.15
Al_2O_3	5.02	4.69	2.33	17.41
Cr_2O_3	5.13	2.50	0.14	0.08
Fe_2O_3	4.78	2.43	2.41	4.75
MnO	0.10	0.06	0.04	0.08
MgO	15.11	15.45	23.05	12.48
CaO	22.90	24.94	17.90	17.14
Na_2O	0.11	0.07	0.15	0.76
K_2O	0.01	0.00	0.01	0.01
P_2O_5	0.01	0.01	0.00	0.00
NiO	0.05	0.04	0.09	0.03
Total	99.64	100.59	101.97	102.15
Cr (in μg/g)*	35099	17105	958	547

Determined by XRF analysis using lithium borate glass beads (see Akizawa et al., submitted)
* Cr abundance was calculated from Cr_2O_3 content of the XRF analytical result.

diopsidite) were separately prepared. A whitish rock sample enveloped in the mantle diopsidite and a crustal gabbro sample were also used in this study. Detailed petrographical features of studied samples were described in Akizawa and Arai (2014), Arai and Akizawa (2014) and Akizawa et al. (submitted). Major-element compositions of whole rocks and minerals were determined by XRF and electron microprobe analyses at Kanazawa University, respectively (Table 1) (see Akizawa et al., submitted). Cr_2O_3 contents of chromite-rich and chromite-poor diopsidite samples are 5.13 wt% and 2.50 wt%, respectively. Chromites in the mantle diopsidite are considerably heterogeneous in composition even in a single grain (Mg#=0.12-0.50 and Cr#=0.58-0.83).

3 Preparation and observation of fused glass

"Whole-rock fused glass" (fused glass) was prepared by a direct fusion method using an iridium-strip heater at Kanazawa University. In-house made copper electrodes connected to a direct current power supply (PK6-130, Matsusada Precision) and an iridium strip (99.85% Ir-foil, Nilaco Corporation) were used for preparation of the fused glass. An aliquot ($\approx$20 mg) of the powdered rock sample was fused on the iridium-strip heater and the fused glass bead was obtained by quenching of the melt. Further details of procedure were described in Tamura et al. (2015 in press).

Four beads of fused glass were prepared from the chromite-rich diopsidite sample and

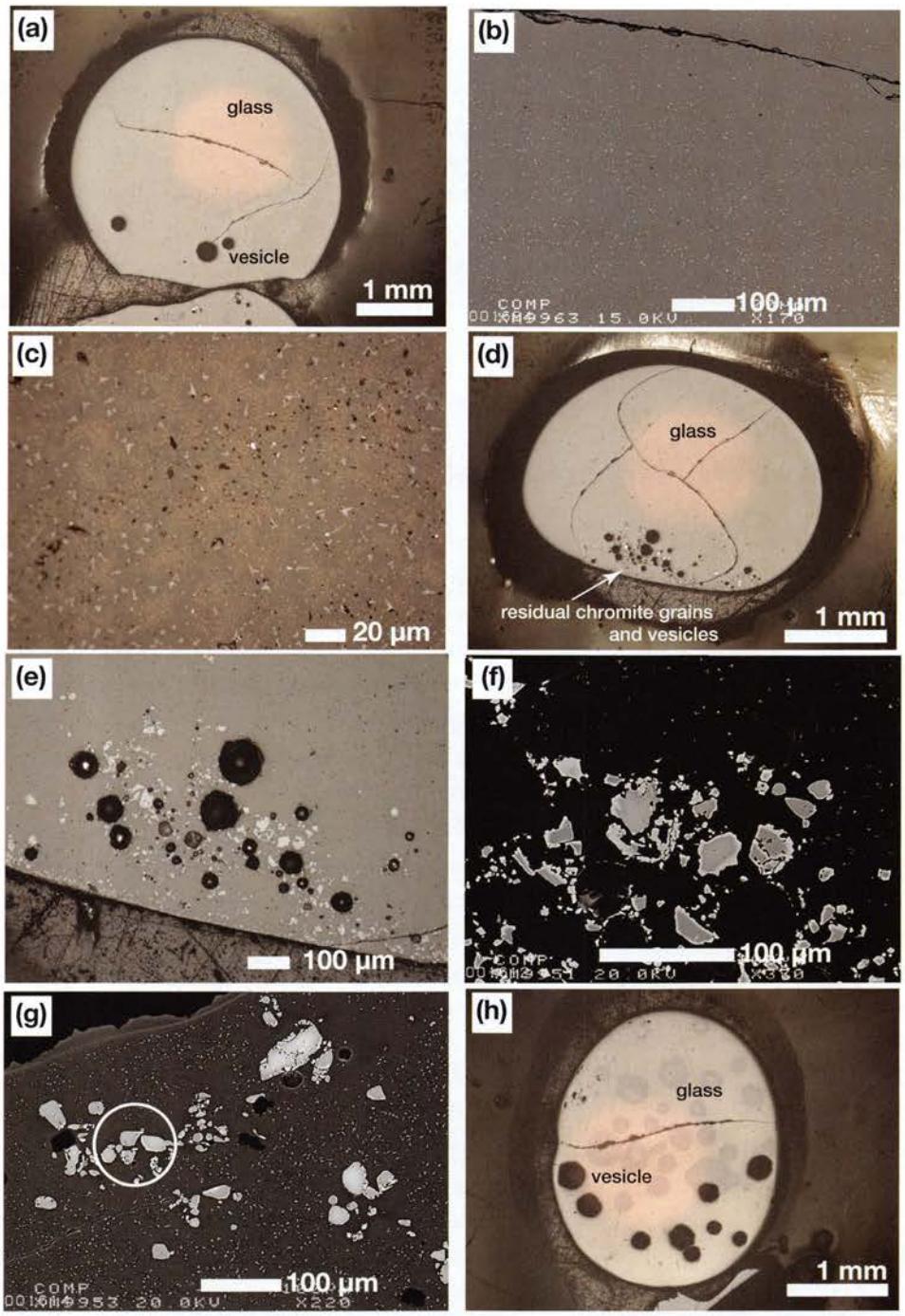

Figure 2. Photomicrographs under reflected light (a, c, d, e and h) and backscattered electron images (b, f, and g) of the polished surface of fused glass prepared from the chromite-rich diopsidite (a-g) and gabbro samples (h). (a) residual chromite grain-free fused glass. Note that star-shaped quench crystals are widely distributed in the fused glass, as shown in (b) and (c). (d) residual chromite grain-bearing fused glass. Closeup of chromite grains is shown in (e) and (f). Note that the chromite grains and vesicles are distributed at rim of the fused glass. (g) another example of the chromite grain-bearing fused glass. Chromite grains are surrounded by quench crystals (fine white dots). The circle indicates an example of an analytical spot (100µm in diameter) composed of glass and residual chromite grains (see Table 2). (h) example of the homogeneous fused glass.

they showed modal heterogeneities in the polished surface (Fig. 2a-g). Quench crystals of micron-scale star-shaped chromite are widely distributed in all the fused glasses (Fig. 2a-c), whereas residual grains of chromite are also observed in three of them (Fig. 2d). Residual chromite grains are generally related to vesicles, and are distributed at rim of the fused glasses. The grains are irregular or equant in shape and relatively coarse (<50 μm in diameter) (Fig. 2e-g). Modal ratio of the grains is approximately <1 vol.% of the fused glass (Fig. 2d). Cr# of residual chromite grains is 0.62-0.85 which is comparable to Cr# of chromite in the mantle diopsidite (Akizawa and Arai, 2014; Arai and Akizawa, 2014; Akizawa et al., submitted). Neither quench crystals nor residual grains are observed in the fused glasses prepared from other samples (Fig. 2h).

4 Analytical procedure and strategy

Trace elements (Sc, Ti, V, Cr, Co, Ni, Rb, Sr, Y, Zr, Nb, Cs, Ba, Hf, Ta, Th, U and REEs) and an internal standard element (Si) of the fused glass were analyzed by LA-ICP-MS (MicroLas GeoLas Q-plus 193 nm ArF excimer laser system and Agilent 7500 s) at Kanazawa University (Morishita et al., 2005). Each analysis was performed by single-spot ablation of 100μm in diameter at 5 Hz repetition rate with energy density of 8 J/cm^2 per pulse. Signal integration times are 50 sec for a gas background interval and 50 sec for a laser ablation interval by 250 pulse shots. Further operation conditions and procedures of LA-ICP-MS analysis were along Tamura et al. (2015 in press).

We carefully examined the heterogeneity of the fused glass beads prepared from the chromite-rich diopsidite sample because they contain the quench crystals and residual grains of chromite (Fig. 2a-g), as described above. Spot diameter of 100μm can not avoid the quench crystals of chromite but can contrastingly obtain the data from the glass with crystals. Two sets of 3-spot analyses randomly selected were carried out on the residual grain-free fused glass. To examine the interference from the quench crystals, the laser-ablation spot size of 30μm was also used in the measurement of the fused glass. To evaluate further interference, residual chromite grains with surrounding glass are selected as one of 3-spot analytical targets (Fig. 2g). This is based on the assuming that the chromite is basically very poor in incompatible elements as well as Si, and such elements can be ignored the interference from the chromite.

BCR-2G was used as the calibration standard material and the reference value of elements was selected from GeoReM database (Jochum and Nohl, 2008). Data reduction was facilitated using internal standard element correction, as followed a protocol essentially identical to that outlined by Longerich et al. (1996), such as,

Table 2. LA–ICP–MS analytical data of the fused glass from studied samples

Rock	Mantle Diopsidite																	
Sample	chromite-rich diopsidite																	
FG	FG#1 (residual chromite grain free)																	
	#101	#102	#103	AVE	RSD		#201	#202	#203	AVE	RSD	AVE*	RSD		#301	#302	#303	AVE	RSD	RD**
(μg/g)															LA30	LA30	LA30			
Sc	17.9	17.5	17.8	17.7	1.2%		17.7	17.7	17.2	17.6	1.7%	17.6	1.4%		15.8	15.9	16.0	15.9	0.8%	0.90
Ti	620	614	617	617	0.5%		606	603	595	602	0.9%	609	1.5%		561	564	582	569	2.0%	0.93
V	202	198	205	202	1.6%		209	213	196	206	4.2%	204	3.1%		198	196	195	196	0.9%	0.96
Cr	33953	28814	36460	33076	11.8%		36081	37916	29705	34567	12.5%	33822	11.1%		37277	31787	33749	34271	8.1%	1.01
Co	107	101	109	106	3.7%		105	108	97	103	5.7%	105	4.5%		106	104	105	105	1.3%	1.00
Ni	397	367	400	388	4.8%		364	378	339	360	5.4%	374	6.1%		470	447	443	454	3.2%	1.21
Sr	12.20	11.67	12.02	11.96	2.2%		11.72	11.85	11.87	11.81	0.7%	11.89	1.6%		11.18	11.46	11.96	11.53	3.4%	0.97
Y	5.26	5.16	5.29	5.24	1.4%		5.31	5.32	5.18	5.27	1.5%	5.255	1.3%		4.45	4.55	4.59	4.53	1.6%	0.86
Zr	12.10	11.86	11.93	11.96	1.0%		12.35	12.39	12.33	12.36	0.2%	12.16	1.9%		10.84	11.27	11.18	11.10	2.0%	0.91
Nb	0.64	0.58	0.65	0.62	5.9%		0.69	0.70	0.60	0.66	8.1%	0.64	7.3%		0.66	0.62	0.62	0.63	3.9%	0.98
Ba	9.83	9.60	9.81	9.75	1.3%		9.37	9.49	10.19	9.68	4.6%	9.72	3.0%		9.09	9.13	9.47	9.23	2.2%	0.95
La	0.354	0.338	0.347	0.346	2.3%		0.334	0.343	0.347	0.341	2.0%	0.344	2.1%		0.315	0.321	0.335	0.324	3.2%	0.94
Ce	1.008	0.970	1.007	0.995	2.2%		1.010	1.046	1.067	1.041	2.8%	1.018	3.3%		1.048	1.031	1.016	1.032	1.6%	1.01
Pr	0.186	0.179	0.184	0.183	2.0%		0.186	0.193	0.194	0.191	2.3%	0.187	3.0%		0.181	0.189	0.183	0.184	2.3%	0.99
Nd	1.091	1.040	1.077	1.069	2.5%		1.091	1.110	1.084	1.095	1.2%	1.082	2.2%		1.049	0.953	1.002	1.001	4.8%	0.93
Sm	0.407	0.382	0.409	0.399	3.8%		0.401	0.432	0.404	0.412	4.1%	0.406	4.0%		0.306	0.283	0.393	0.327	17.7%	0.81
Eu	0.161	0.151	0.163	0.158	4.1%		0.163	0.156	0.160	0.160	2.2%	0.159	2.9%		0.178	0.141	0.162	0.160	11.6%	1.01
Gd	0.563	0.554	0.565	0.561	1.0%		0.565	0.573	0.572	0.570	0.8%	0.565	1.2%		0.438	0.476	0.532	0.482	9.8%	0.85
Tb	0.103	0.097	0.104	0.101	3.7%		0.104	0.103	0.105	0.104	1.0%	0.103	2.8%		0.096	0.105	0.104	0.102	4.9%	0.99
Dy	0.760	0.729	0.758	0.749	2.3%		0.800	0.797	0.774	0.790	1.8%	0.770	3.5%		0.644	0.634	0.725	0.668	7.5%	0.87
Ho	0.171	0.167	0.171	0.170	1.4%		0.172	0.180	0.172	0.175	2.6%	0.172	2.5%		0.129	0.150	0.167	0.149	12.8%	0.86
Er	0.591	0.588	0.582	0.587	0.8%		0.605	0.621	0.591	0.606	2.5%	0.596	2.4%		0.510	0.491	0.550	0.517	5.8%	0.87
Tm	0.100	0.096	0.102	0.099	3.1%		0.103	0.098	0.104	0.102	3.2%	0.101	3.1%		0.076	0.089	0.101	0.089	14.1%	0.88
Yb	0.878	0.840	0.876	0.865	2.5%		0.888	0.882	0.853	0.874	2.1%	0.870	2.2%		0.744	0.743	0.795	0.761	3.9%	0.87
Lu	0.245	0.241	0.241	0.242	1.0%		0.254	0.250	0.246	0.250	1.6%	0.246	2.1%		0.236	0.233	0.247	0.239	3.1%	0.97
Hf	0.390	0.371	0.410	0.390	5.0%		0.408	0.402	0.397	0.402	1.4%	0.396	3.6%		0.327	0.252	0.289	0.289	13.0%	0.73
Ta	0.045	0.044	0.045	0.045	1.3%		0.042	0.046	0.045	0.044	4.7%	0.045	3.1%		0.034	0.047	0.043	0.041	16.1%	0.93
Th	0.217	0.211	0.218	0.215	1.8%		0.230	0.228	0.220	0.226	2.3%	0.221	3.2%		0.163	0.181	0.166	0.170	5.7%	0.77
U	0.019	0.017	0.017	0.018	6.5%		0.017	0.019	0.018	0.018	5.6%	0.018	5.5%		0.015	0.012	0.021	0.016	28.6%	0.90

FG: fused glass. 4 fused glass beads (FG#1–#4) were prepared from the chromite–rich diopsidite sample. 3 sets of 3–spot data were obtained from the single chromite grain–free fused glass.
AVE: mean value of 3–spot analyses, RSD: relative standard deviation (1σ),
AVE*: averaged value of 6–spot data, RD**: relative deviation to AVE*.
LA30: 30 μm spot size used.

$$\left(\frac{IE_{signal}}{IE_{conc}}\right)_{EXTSTD} : \left(\frac{IE_{signal}}{IE_{conc}}\right)_{sample} = \left(\frac{X_{signal}}{X_{conc}}\right)_{EXTSTD} : \left(\frac{X_{signal}}{X_{conc}}\right)_{sample} \quad \cdots\cdots \text{Eq. 1.}$$

Here, IE_{signal} and X_{signal} are signal intensities of an internal standard element and other elements, respectively, whereas IE_{conc} and X_{conc} are concentrations of each element in the measurement of calibration standard material (EXTSTD) and unknown material (sample). In this study, SiO_2 concentration determined by the XRF analysis (Table 1)

Table 2. (continued)

Rock	Mantle Diopsidite														
Sample	chromite-rich diopsidite														
FG	FG#2 (residual chromite grain bearing)					FG#3 (residual chromite grain bearing)					FG#4 (residual chromite grain bearing)				
	#1–1	#1–2	#1–3	AVE	RSD	#2–1	#2–2	#2–3	AVE	RSD	#3–1	#3–2	#3–3	AVE	RSD
(μg/g)	chromite***					chromite***					chromite***				
Sc	19.8	18.2	18.0	18.7	5.2%	16.9	17.5	18.7	17.7	5.2%	17.3	17.4	18.1	17.6	2.5%
Ti	839	782	661	761	11.9%	452	464	745	554	29.9%	456	448	584	496	15.4%
V	338	208	202	249	30.9%	192	196	381	256	42.3%	191	188	278	219	23.3%
Cr	171690	29782	31441	77638	104.9%	33223	34305	122002	63177	80.6%	32910	32650	93694	53085	66.3%
Co	188	108	102	132	36.1%	98	101	174	124	34.7%	96	97	137	110	21.5%
Ni	722	388	380	497	39.2%	342	355	610	436	34.8%	356	355	485	399	18.7%
Sr	12.01	14.63	13.07	13.24	9.9%	8.02	8.35	8.40	8.26	2.5%	8.15	8.22	8.18	8.18	0.4%
Y	5.48	5.52	5.42	5.47	0.9%	4.82	5.02	5.07	4.97	2.7%	4.99	5.03	5.03	5.02	0.5%
Zr	13.65	14.20	12.62	13.49	5.9%	10.03	10.37	11.33	10.58	6.4%	10.35	10.29	11.18	10.61	4.7%
Nb	1.97	0.72	0.65	1.11	66.3%	0.54	0.54	1.47	0.85	63.3%	0.53	0.52	1.18	0.74	50.8%
Ba	10.61	16.79	12.34	13.24	24.1%	2.65	2.72	2.67	2.68	1.4%	2.60	2.66	2.65	2.64	1.2%
La	0.397	0.620	0.433	0.483	24.8%	0.107	0.101	0.106	0.105	3.1%	0.096	0.097	0.099	0.097	1.6%
Ce	1.076	1.528	1.167	1.257	19.0%	0.522	0.508	0.534	0.521	2.5%	0.514	0.524	0.508	0.515	1.6%
Pr	0.195	0.253	0.208	0.219	13.9%	0.122	0.120	0.122	0.121	1.0%	0.122	0.123	0.123	0.123	0.5%
Nd	1.182	1.368	1.164	1.238	9.1%	0.795	0.807	0.807	0.803	0.9%	0.815	0.819	0.798	0.811	1.4%
Sm	0.410	0.467	0.414	0.430	7.4%	0.337	0.343	0.356	0.345	2.8%	0.339	0.359	0.333	0.344	4.0%
Eu	0.157	0.175	0.163	0.165	5.6%	0.135	0.144	0.139	0.139	3.2%	0.144	0.149	0.140	0.144	3.1%
Gd	0.583	0.583	0.563	0.576	2.0%	0.468	0.490	0.497	0.485	3.1%	0.494	0.501	0.523	0.506	3.0%
Tb	0.108	0.111	0.110	0.110	1.4%	0.093	0.099	0.102	0.098	4.7%	0.093	0.095	0.093	0.094	1.2%
Dy	0.781	0.821	0.762	0.788	3.8%	0.684	0.718	0.754	0.719	4.9%	0.722	0.729	0.723	0.725	0.5%
Ho	0.172	0.184	0.179	0.178	3.4%	0.157	0.151	0.166	0.158	4.8%	0.155	0.151	0.161	0.156	3.2%
Er	0.603	0.625	0.596	0.608	2.5%	0.543	0.564	0.569	0.559	2.5%	0.557	0.563	0.589	0.570	3.0%
Tm	0.104	0.103	0.101	0.103	1.5%	0.093	0.097	0.098	0.096	2.8%	0.099	0.097	0.095	0.097	2.1%
Yb	0.877	0.868	0.870	0.872	0.5%	0.785	0.841	0.848	0.825	4.2%	0.821	0.814	0.847	0.827	2.1%
Lu	0.253	0.314	0.235	0.267	15.5%	0.183	0.211	0.208	0.201	7.7%	0.204	0.211	0.218	0.211	3.3%
Hf	0.374	0.426	0.370	0.390	8.0%	0.299	0.323	0.289	0.304	5.8%	0.304	0.304	0.299	0.302	1.0%
Ta	0.036	0.067	0.039	0.047	36.1%	0.021	0.021	0.022	0.021	2.7%	0.022	0.023	0.025	0.023	6.5%
Th	0.226	0.302	0.239	0.256	15.9%	0.157	0.156	0.155	0.156	0.6%	0.163	0.160	0.163	0.162	1.1%
U	0.022	0.015	0.019	0.019	18.8%	0.024	0.021	0.020	0.022	9.6%	0.021	0.022	0.022	0.022	2.7%

***spot analysis of the glass including residual chromite grains. An example spot (#2–3) is shown in Figure 2g.

was used as the internal standard element value of the sample [$(IE_{conc})_{sample}$]. Given reference compositions of the calibration standard material, an element concentration in the sample [$(X_{conc})_{sample}$] can be calculated. Results of the measurement are listed in Tables 2.

Table 2. (continued)

Rock	Mantle Diopsidite										Whitish Rock					Gabbro				
Sample	chromite-poor diopsidite					chromite-poor diopsidite														
FG	FG#1					FG#2					FG#1					FG#1				
	#1–1	#1–2	#1–3	AVE	RSD	#2–1	#2–2	#2–3	AVE	RSD	#1–1	#1–2	#1–3	AVE	RSD	#1–1	#1–2	#1–3	AVE	RSD
(μg/g)																				
Sc	15.3	15.5	16.1	15.6	2.5%	15.5	15.6	15.5	15.5	0.3%	10.2	10.2	10.2	10.2	0.1%	39.1	40.0	41.3	40.1	2.7%
Ti	353	360	368	360	2.0%	370	372	361	368	1.6%	374	373	379	375	0.8%	931	947	973	950	2.2%
V	126	131	131	129	2.1%	136	136	134	135	0.9%	66	65	66	66	0.8%	116	119	119	118	1.8%
Cr	17267	17842	17929	17679	2.0%	19344	19023	19818	19395	2.1%	1275	1239	1297	1270	2.3%	470	478	516	488	5.0%
Co	49	51	50	50	2.3%	53	53	55	54	1.9%	32	31	32	32	1.4%	50	51	50	50	1.1%
Ni	270	280	276	275	1.9%	286	285	296	289	2.1%	643	623	629	632	1.6%	175	183	178	178	2.4%
Sr	8.31	8.47	8.43	8.40	1.0%	8.59	8.50	8.66	8.58	0.9%	10.69	10.79	10.89	10.79	0.9%	105.79	103.81	103.42	104.34	1.2%
Y	5.35	5.42	5.51	5.43	1.5%	5.40	5.32	5.33	5.35	0.8%	4.81	4.80	4.89	4.83	1.0%	4.15	4.30	4.47	4.31	3.8%
Zr	13.41	13.54	13.86	13.61	1.7%	13.51	13.53	13.50	13.51	0.1%	5.84	5.82	5.88	5.85	0.6%	1.70	1.73	1.99	1.81	8.9%
Nb	0.41	0.42	0.44	0.42	3.9%	0.42	0.44	0.45	0.43	3.1%	0.21	0.20	0.21	0.21	2.5%	0.02	0.02	0.03	0.02	25.6%
Ba	6.32	6.61	6.64	6.52	2.7%	6.75	6.69	6.79	6.74	0.7%	9.08	9.13	9.51	9.24	2.5%	5.09	4.92	5.48	5.16	5.6%
La	0.133	0.142	0.141	0.139	3.6%	0.149	0.141	0.147	0.146	2.9%	0.514	0.511	0.526	0.517	1.5%	0.119	0.114	0.126	0.120	5.0%
Ce	0.628	0.658	0.634	0.640	2.5%	0.665	0.646	0.663	0.658	1.6%	2.160	2.180	2.217	2.186	1.3%	0.432	0.431	0.461	0.441	3.9%
Pr	0.147	0.152	0.154	0.151	2.4%	0.154	0.151	0.156	0.154	1.6%	0.366	0.379	0.374	0.373	1.8%	0.102	0.095	0.102	0.100	4.1%
Nd	0.950	0.967	1.014	0.977	3.4%	0.984	0.974	1.004	0.987	1.5%	1.740	1.789	1.815	1.781	2.1%	0.676	0.679	0.728	0.694	4.2%
Sm	0.376	0.403	0.397	0.392	3.6%	0.381	0.376	0.369	0.375	1.6%	0.503	0.494	0.512	0.503	1.8%	0.338	0.354	0.371	0.354	4.7%
Eu	0.186	0.195	0.191	0.191	2.4%	0.190	0.187	0.190	0.189	0.9%	0.136	0.136	0.140	0.137	1.7%	0.223	0.222	0.228	0.224	1.4%
Gd	0.562	0.579	0.575	0.572	1.6%	0.563	0.562	0.579	0.568	1.7%	0.607	0.602	0.615	0.608	1.1%	0.589	0.577	0.627	0.598	4.4%
Tb	0.110	0.108	0.111	0.110	1.4%	0.107	0.104	0.107	0.106	1.6%	0.108	0.109	0.104	0.107	2.5%	0.108	0.110	0.126	0.115	8.6%
Dy	0.755	0.764	0.787	0.769	2.1%	0.755	0.771	0.753	0.760	1.3%	0.717	0.728	0.744	0.730	1.9%	0.776	0.778	0.824	0.793	3.4%
Ho	0.166	0.167	0.179	0.171	4.2%	0.170	0.166	0.174	0.170	2.4%	0.154	0.161	0.159	0.158	2.3%	0.166	0.168	0.175	0.170	2.8%
Er	0.590	0.592	0.610	0.597	1.8%	0.588	0.574	0.592	0.585	1.6%	0.514	0.513	0.533	0.520	2.2%	0.493	0.487	0.512	0.497	2.6%
Tm	0.098	0.101	0.102	0.100	2.1%	0.105	0.099	0.099	0.101	3.4%	0.080	0.084	0.082	0.082	2.4%	0.064	0.065	0.066	0.065	1.5%
Yb	0.863	0.885	0.888	0.879	1.6%	0.887	0.859	0.889	0.878	1.9%	0.587	0.593	0.611	0.597	2.1%	0.439	0.417	0.462	0.439	5.1%
Lu	0.207	0.214	0.217	0.213	2.4%	0.259	0.256	0.253	0.256	1.2%	0.099	0.099	0.104	0.101	2.9%	0.093	0.100	0.102	0.098	4.8%
Hf	0.536	0.572	0.551	0.553	3.3%	0.556	0.534	0.558	0.549	2.4%	0.141	0.146	0.142	0.143	1.9%	0.086	0.093	0.105	0.095	10.2%
Ta	0.020	0.023	0.023	0.022	7.9%	0.031	0.033	0.032	0.032	3.1%	0.023	0.026	0.027	0.025	8.2%	0.019	0.014	0.021	0.018	20.0%
Th	0.280	0.300	0.303	0.294	4.2%	0.285	0.282	0.289	0.285	1.2%	0.100	0.097	0.101	0.099	2.1%	0.004	0.004	0.006	0.005	24.7%
U	0.043	0.039	0.042	0.041	5.0%	0.038	0.039	0.038	0.038	1.5%	0.019	0.017	0.021	0.019	10.5%	0.001	0.000	0.001	0.001	86.6%

2 fused glass beads (FG#1 and #2) were prepared from the chromite-poor diopsidite sample.

5 Results and Discussion

5.1 Homogeneous fused glass

Our previous study demonstrated that the routine measurement work, such as 3-spot analyses randomly selected on the fused glass by LA-ICP-MS, can reproduce the whole-rock trace-element compositions of the geological reference materials (Tamura et al., 2015 in press). Trace elements especially useful for the petrological study, such as REE, LILE and HFSE, were well reproduced within 10% offset from the reference values (Fig.

1). The study also indicated that the routine work can provide the reliable data for Cr of 150-2200μg/g (with 15% uncertainty). However, analytical data of some elements are not accurate because of the volatilization (Pb and U) or contamination (Lu, Hf and Ta) during preparation of the fused glass.

Fused glass beads from samples of chromite-poor diopsidite, whitish rock and gabbro are modally homogeneous (e.g., Fig. 2h). High precision data (better than 5% relative

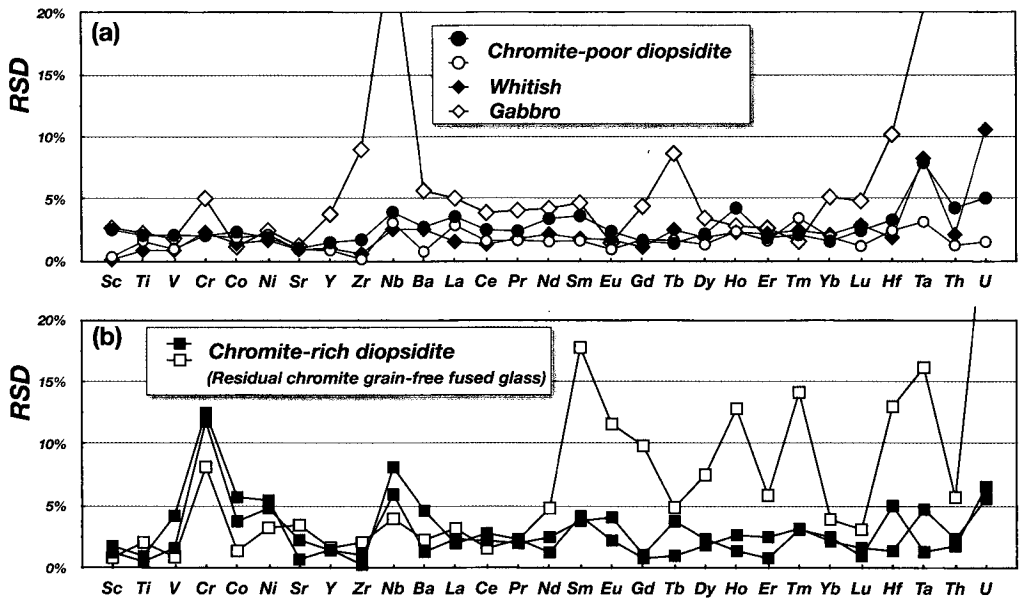

Figure 3. Precision of 3-spot LA-ICP-MS analytical data of the fused glass of studied samples. RSD is relative standard deviation (1σ). (a) chromite-poor diopsidite (2 fused glass beads), whitish rock and gabbro samples. (b) chromite-rich diopsidite sample. 2 sets of 3-spot analyses were carried out on a bead of the single residual chromite grain-free fused glass (closed square). Open square indicates analytical data using a spot size of 30μm (see text).

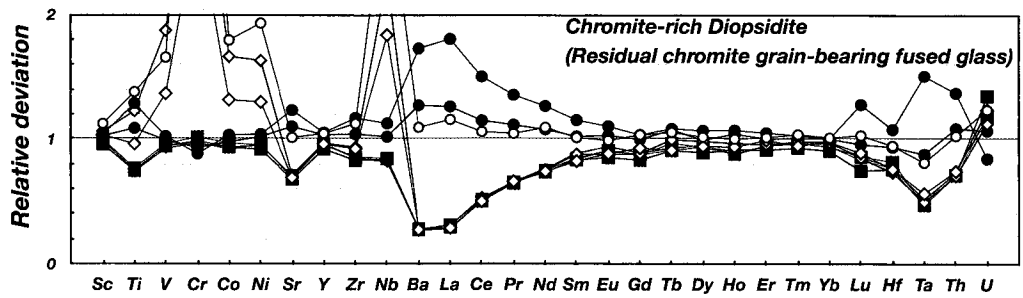

Figure 4. Comparison of LA-ICP-MS data between fused glass beads of the chromite-rich diopsidite sample. Relative deviation between each spot result in 3 beads of the residual chromite grain-bearing fused glass and averaged value of 6-spot analysis of the residual grain-free fused glass. Closed symbols are data from the analytical spot away from residual chromite grains. Open symbols are data from the analytical spot composed of glass and residual chromite grains (e.g. Fig. 2g) (see text).

standard deviation: RSD) of 3-spot analyses of such samples support that the fused glass beads are elementally homogeneous (Fig. 3a). Based on the accuracy shown in our previous study (Fig. 1), the measurement data for many elements are reliable within 10% uncertainty. Cr data of the samples are in good agreement with those obtained in advance with XRF (Tables 1 and 2).

In contrast, fused glass beads of the chromite-rich diopsidite sample are heterogeneous in terms of the abundance of quench crystals and residual grains of chromite (Fig. 2a-h). This is probably due to the extremely high Cr contents (Cr_2O_3=5 wt%) and abundant chromite grains in the sample (Akizawa and Arai, 2014; Arai and Akizawa, 2014; Akizawa et al., submitted). The precision of Cr data is better than 11% RSD (Fig. 3b) despite such frequent distribution of the quench crystal in the residual chromite grain-free fused glass bead. This indicates that quench crystals are so minute in size and so evenly distributed in the fused glass that their presence can be ignored practically. Cr data from the mean value of 3-spot analyses match with the results of the XRF analysis within 5% offset (Tables 1 and 2). The homogeneity of the fused glass is also supported by other trace-element data with high precision (< 5% RSD) (Fig. 3b). Therefore, we suggest that the LA-ICP-MS analysis of the residual grain-free fused glass is reliable enough to represent whole-rock compositions of the chromite-rich diopsidite sample. However, the compositions are also in good agreement in many incompatible elements with the LA-ICP-MS analytical results of residual chromite grain -bearing fused glass beads (Fig. 4). In following sections, we discuss the reliability and uncertainty of the results based on the data of the heterogeneous fused glass.

5.2 Residual chromite-bearing fused glass

In the data reduction of LA-ICP-MS analysis, the internal standard element calibrates the difference of ablated volumes between samples and the external standard material (Eq1; Longerich et al., 1996). The reduction process theoretically allows to use different laser-ablation spot sizes between them. Although the target spot is composed of the glass and residual chromite grains, the incompatible-element abundance can be estimated as a whole-rock composition if the SiO_2 content of internal standard element is given. Chromite grains are considered as blank for Si and incompatible elements, and this situation is equivalent to analyses using different spot sizes between sample and the external standard material.

Residual chromite grains are mainly distributed at rim of each fused glass bead, where vesicles are also concentrated (Fig. 2d-f). Analytical spots on the glass and residual chromite grains (e.g., Fig. 2g) yielded 3-5 times higher Cr abundance than spots away from the residual grains and spots of the residual chromite grain-free glass (Fig. 5). Such a high-Cr abundance is clearly due to interference from chromite grains both in the

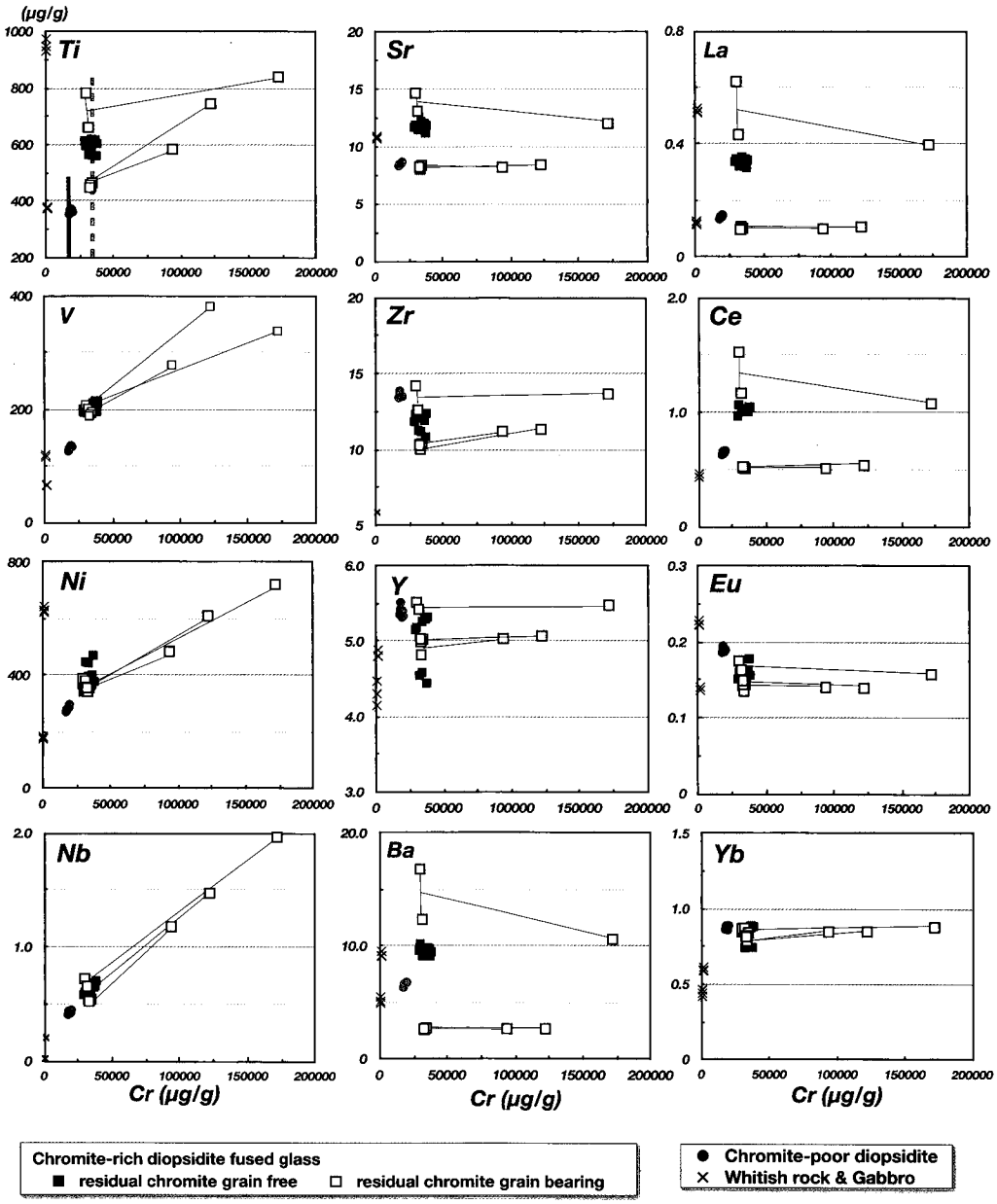

Figure 5. Relationships between Cr and selected trace-element data. High-Cr abundance data are from the analytical spot composed of the glass and residual chromite grains in 3 fused glass beads, and 3-spot data of each glass bead are tied by lines. XRF data of Cr in chromite-rich and chromite-poor diopsidite samples are shown by broken line and bold line, respectively, in the first panel. Note that the high Nb abundance may result not only from the contamination of chromitite but also from mass interference to ^{93}Nb from $^{53}Cr^{40}Ar$ caused by abundant Cr.

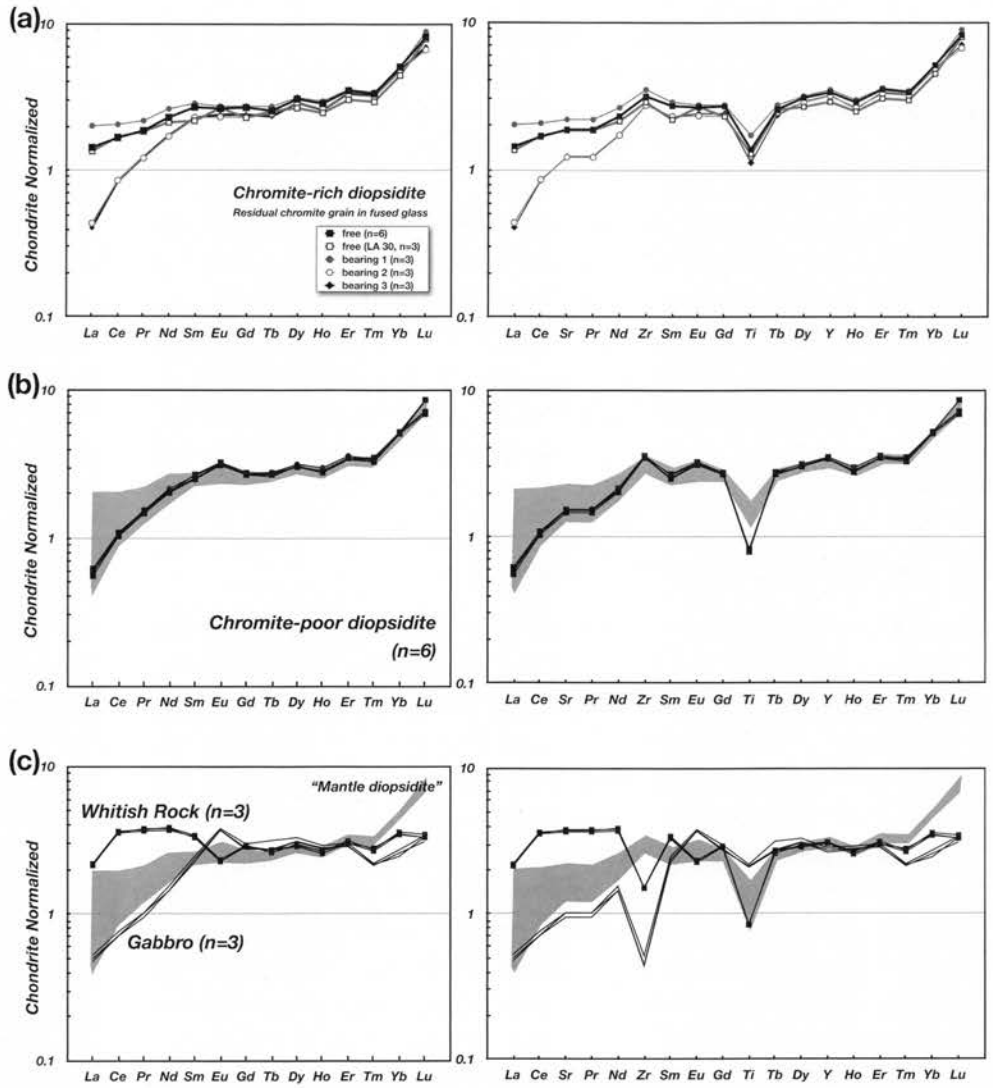

Figure 6. Chondrite normalized REE (left) and trace-element patterns (right) of studied samples. Averaged data of each fused glass bead of the chromite-rich diopsidite (a) and all spot data of other samples (b and c) are shown. n is number of the spot analysis. Shaded area in (b) shows compositional range of (a). Field of "mantle diopside" in (c) indicates the compositional range of (a) and (b) (see text). Lu abundance is highly uncertain based on our previous study (see Tamura et al., 2015 in press). Chondrite normalized values are from Sun and McDonough (1989).

calibration and in the analysis. The variation of Cr abundance mainly depends on the proportion between chromite and glass in the analytical spot. As shown in Figure 5, in each fused glass bead, abundances of some elements (e.g., Ti, V, Ni and Nb) are also higher in the analytical spot with residual chromite grains than in the other spots. This

indicates that the chromite grains interfere with the measurement of these elements. On the other hand, results of representative incompatible elements (e.g., Sr, Zr, Y, Ba and REE) are unrelated to the chromite contamination. The analytical data of the residual chromite grain-bearing spot are almost equivalent to those of other 2 spots in each fused glass bead (Fig. 5). The results are consistent with compositions of chromite which is so poor in such incompatible elements and SiO_2 that we safely ignore the interference. Remarkable heterogeneities in Sr, Ba and light-REE (LREE) are observed in one of the glass beads (up to 25 % RSD) (Fig. 5 and Table 2). However, discrepancies of these element data between 4 fused glass beads of the chromite-rich diopsidite sample are more substantial than the heterogeneity (Fig. 5). If our results, such as the averaged value of 3-spot analytical data, represent the compositions of the fused glass bead at least, the discrepancies should be discussed in order to use them as geochemical data of the sample (Fig. 4).

5.3 Reliability as geochemical data

Chondrite normalized REE and incompatible trace-element patterns of our samples are summarized in Figure 6. Compositional characteristics are distinguished for each sample and are helpful for petrological discussion. However, the patterns apparently show the discrepancies in LREE between four fused glass beads of the chromite-rich diopsidite sample (Figs. 6a). Two fused glass beads including the residual chromite grain-free glass bead are rich in Sr and LREE relative to other two fused glass beads (Fig. 6a). The trace-element patterns of the latter ones are indistinguishable from those of the chromite -poor diopsidite sample although Cr abundance are clearly different between them (Figs. 5 and 6b). No correlation between incompatible-element and Cr abundances (Fig. 5) supports that the variations of the patterns are mainly controlled by silicate minerals rather than chromite. Such silicate minerals in the aliquot of whole-rock powders could be more heterogeneous in the chromite-rich diopsidite sample than in the chromite-poor sample because the proportion of silicate minerals is relatively low in the aliquot of the chromite-rich sample. Considering the modal characteristics of the sample, therefore, we speculate that compositional variations of Sr and LREE were caused by differences between powdered aliquots to use for preparing the fused glass rather than by heterogeneity in the fused glass.

Our analyses and results presented here are not critical to distinguish incompatible-element compositions of the chromite-rich diopsidite from those of the chromite-poor diopsidite. Therefore, as shown in Figure 6c, both data should be convergently used as compositions of "mantle diopsidite" for our petrological study. As demonstrated by LA-ICP-MS and XRF analyses, in contrast, the modal heterogeneity of chromite in mantle diopsidite is well reflected by the difference of Cr abundance between them.

6 Conclusions

Whole-rock trace-element compositions of mantle diopsidite and related rock samples were determined by the the flux-free fused glass and LA-ICP-MS analysis. Chromite-rich and -poor portions of the mantle diopsidite were separately examined. Measurements for the chromite-bearing heterogeneous fused glass as well as the homogeneous glass revealed that reliable data of the incompatible elements can be obtained by the analysis on even target spots including residual grains and/or quench crystals of chromite. However, our results indicated that the compositions are indistinguishable between chromite-rich and chromite-poor diopsidite samples. In petrological studies, therefore, the incompatible-element compositions should be discussed as the geochemical data of "mantle diopsidite".

Acknowledgements

This manuscript was improved by constructive comments from an anonymous reviewer. We thank A. Matsuki for the editorial handling. The electrodes were constructed by Technical Support Center, Kanazawa university. We thank S. Umino and T. Morishita for their technical advice.

References

Akizawa, N. and Arai, S. (2014) Petrology of mantle diopsidite from Wadi Fizh, northern Oman ophiolite: Cr and REE mobility by hydrothermal solution. Island Arc, v. 23, p. 312-323.

Akizawa, N., Arai, S., Tamura, A. and Python, M. (submitted) Hydrothermal circulation around suboceanic Moho beneath the first-spreading ridge: an example of diopsidite and anorthosite formation in Wadi Fizh, Oman ophiolite. Submitted to Lithos.

Arai, S. and Akizawa, N. (2014) Precipitation and dissolution of chromite by hydrothermal solutions in the Oman ophiolite: New behavior of Cr and chromite. American Mineralogist, v. 99, p. 28-34.

Eggins, S., Rudnick, R. L. and McDonough, W. F. (1998) The composition of peridotites and their minerals: a laser-ablation ICP-MS study. Earth and Planetary Science Letters, v. 154, p. 53-71.

Eggins, S. M., Woodhead, J. D., Kinsley, L. P. J., Mortimer, G. E., Sylvester, P., McCulloch, M. T., Hergt, J. M. and Handler, M. R. (1997) A simple method for the precise determination of > 40 trace elements in geological samples by ICPMS using enriched isotope internal standardisation. Chemical Geology, v. 134, p. 311-326.

Eggins, S. M. (2003) Laser Ablation ICP-MS Analysis of Geological Materials Prepared as Lithium Borate Glasses. Geostandards Newsletter, v. 27, p. 147-162.

Fedorowich, J. S., Richards, J. P., Jain, J. C., Kerrich, R. and Fan, J. (1993) A rapid method for REE and trace-element analysis using laser sampling ICP-MS on direct fusion whole-rock glasses. Chemical Geology, v. 106, p. 229-249.

Garbe-Schonberg, D. and Muller, S. (2014) Nano-particulate pressed powder tablets for LA-ICP-MS. Journal of Analytical Atomic Spectrometry, v. 29, p. 990-1000.

Hirano, N., machida, S., Abe, N., Morishita, T., Tamura, A. and Arai, S. (2013) Petit-spot lava fields off the central Chile trench induced by plate flexure. Geochemical Journal, v. 47, p. 249-257.

Ito, K., Hasebe, N., Sumita, R., Arai, S., Yamamoto, M., Kashiwaya, K. and Ganzawa, Y. (2009) LA-ICP-MS analysis of pressed powder pellets to luminescence geochronology. Chemical Geology, v. 262, p. 131-137.

Jarvis, K. E. and Williams, J. G. (1993) Laser ablation inductively coupled plasma mass spectrometry (LA-ICP-MS): a rapid technique for the direct, quantitative determination of major, trace and rare-earth elements in geological samples. Chemical Geology, v. 106, p. 251-262.

Jochum, K.P., Dingwell, D.B., Rocholl, A., Stoll, B et al. (2000) The preparation and preliminary characterisation of eight geological MPI-DING reference glasses for in-situ microanalysis. Geostandards Newsletter, v. 24, p. 87-133.

Jochum, K. P. and Nohl, U. (2008) Reference materials in geochemistry and environmental research and the GeoReM database. Chemical Geology, v. 253, p. 50-53.

Longerich, H. P., Jackson, S. E. and Gunther, D. (1996) Laser ablation inductively coupled plasma mass spectrometric transient signal data acquisition and analyte concentration calculation. Journal of Analytical Atomic Spectrometry, v. 11, p. 899-904.

Mason, P. R. D., Jarvis, K. E., Downes, H. and Vannucci, R. (1999) Determination of Incompatible Trace Elements in Mantle Clinopyroxenes by LA-ICP-MS: A Comparison of Analytical Performance with Established Techniques. Geostandards and Geoanalytical Research, v. 23, p. 157-172.

Morishita, T., Ishida, Y., Arai, S. and Shirasaka, M. (2005) Determination of multiple trace element compositions in thin (< 30μm) layers of NIST SRM 614 and 616 using laser ablation-inductively coupled plasma-mass spectrometry. Geostandards and Geoanalytical Research, v. 29, p. 107-122.

Nehring, F., Jacob, D. E., Barth, M. G. and Foley, S. F. (2008) Laser-ablation ICP-MS analysis of siliceous rock glasses fused on an iridium strip heater using MgO dilution. Microchimica Acta, v. 160, p. 153-163.

Orihashi, Y. and Hirata, T. (2003) Rapid quantitative analysis of Y and REE abundances in XRF glass bead for selected GSJ reference rock standards using Nd-YAG 266 nm UV laser ablation ICP-MS. Geochemical Journal, v. 37, p. 401-412.

Pearce, J. A. (2008) Geochemical fingerprinting of oceanic basalts with applications to ophiolite classification and the search for Archean oceanic crust. Lithos, v. 100, p. 14-48.

Shaw, D. M. (2006) Trace Elements in Magmas A Theoretical Treatment. Cambridge University Press, New York, 243 pp

Stoll, B., Jochum, K. P., Herwig, K., Amini, M., Flanz, M., Kreuzburg, B., Kuzmin, D., Willbold, M. and Enzweiler, J. (2008) An Automated Iridium-Strip Heater for LA-ICP-MS Bulk Analysis of Geological Samples. Geostandards and Geoanalytical Research, v. 32, p. 5-26.

Sun, S. S. and McDonough, W. F. (1989) Chemical and isotopic systematics of oceanic basalts: implications for mantle composition and processes. In: A. D. Saunders and M. J. Norry (Eds.) Geological Society Special Publication 42. Magmatism in the Ocean Basins. London: Geological Society, p. 313-345.

Sylvester, P. (2001a) Laser-Ablation-ICPMS in the Earth Sciences: Principles and applications. Mineralogical Association of Canada Short Course Series, 29. Mineralogical Association of Canada, Ottawa, 244 pp

Sylvester, P. (2001b) Trace element analysis of fused whole rock glasses by laser-ablation ICPMS. In: P. Sylvester (Ed.) Short Course Series 29. Laser-ablation-ICPMS in the Earth Sciences: Principles and Applications. Ottawa: Mineralogical Association of Canada, p. 147-162.

Tamura, A., Akizawa, N., Otsuka, R., Kanayama, K., Python, M., Morishita, T. and Arai, S. (2015 in press) Measurement of whole-rock trace-element composition by flux-free fused glass and LA-ICP-MS: evaluation of simple and rapid routine work. Geochemical Journal. v. 49.

Tamura, A., Arai, S., Ishimaru, S. and Andal, E. (2008) Petrology and geochemistry of peridotites from IODP Site U1309 at Atlantis Massif, MAR 30°N: micro- and macro-scale melt penetrations into peridotites. Contributions to Mineralogy and Petrology, v. 155, p. 491-509.

Zhu, L., Liu, Y., Hu, Z., Hu, Q., Tong, X., Zong, K., Chen, H. and Gao, S. (2013) Simultaneous Determination of Major and Trace Elements in Fused Volcanic Rock Powders Using a Hermetic Vessel Heater and LA-ICP-MS. Geostandards and Geoanalytical Research, v. 37, p. 207-229.